

Membrane-dependent oligomeric structure and pore formation of a {beta}-hairpin antimicrobial peptide in lipid bilayers from solid-state NMR

Rajeswari Mani, Sarah D. Cady, Ming Tang, Alan J. Waring, Robert I. Lehrer, and Mei Hong

PNAS published online Oct 23, 2006;

doi:10.1073/pnas.0605079103

This information is current as of October 2006.

Supplementary Material

Supplementary material can be found at:
www.pnas.org/cgi/content/full/0605079103/DC1

This article has been cited by other articles:
www.pnas.org#otherarticles

E-mail Alerts

Receive free email alerts when new articles cite this article - sign up in the box at the top right corner of the article or [click here](#).

Rights & Permissions

To reproduce this article in part (figures, tables) or in entirety, see:
www.pnas.org/misc/rightperm.shtml

Reprints

To order reprints, see:
www.pnas.org/misc/reprints.shtml

Notes:

Membrane-dependent oligomeric structure and pore formation of a β -hairpin antimicrobial peptide in lipid bilayers from solid-state NMR

Rajeswari Mani*, Sarah D. Cady*, Ming Tang*, Alan J. Waring[†], Robert I. Lehrer[†], and Mei Hong**

*Department of Chemistry, Iowa State University, Ames, IA 50011; and [†]Department of Medicine, University of California School of Medicine, Los Angeles, CA 90095

Edited by Ann E. McDermott, Columbia University, New York, NY, and approved September 6, 2006 (received for review June 17, 2006)

We used solid-state NMR spectroscopy to investigate the oligomeric structure and insertion of protegrin-1 (PG-1), a β -hairpin antimicrobial peptide, in lipid bilayers that mimic either the bacterial inner membrane [palmitoyloleoylphosphatidyl ethanolamine and palmitoyloleoylphosphatidylglycerol (POPE/POPG) bilayers] or the red blood cell membrane [neutral palmitoyloleoylphosphatidylcholine (POPC)/cholesterol bilayers]. ¹H spin diffusion from lipids to the peptide indicates that PG-1 contacts both the lipid acyl chains and the headgroups in the anionic membrane but resides far from the lipid chains in the POPC/cholesterol bilayer. ¹⁹F spin diffusion data indicates that 75% of the β -hairpins have homodimerized N strands and C strands in the anionic membrane. The resulting (NCCN)_n multimer suggests a membrane-inserted β -barrel enclosing a water pore. The lipids surrounding the β -barrel have high orientational disorder and chain upturns, thus they may act as fillers for the pore. These results revise several features of the toroidal pore model, first proposed for magainin and subsequently applied to PG-1. In the POPC/cholesterol membrane, the N and C strands of PG-1 cluster into tetramers, suggesting the formation of β -sheets on the membrane surface. Thus, the membrane composition plays a decisive role in defining the assembly and insertion of PG-1. The different oligomeric structures of PG-1 help to explain its greater toxicity for bacteria than for eukaryotic cells.

membrane composition | spin diffusion | toroidal pores | ¹⁹FNMR | protegrin-1

Antimicrobial peptides (AMPs) are part of the innate immune system of many animals and plants (1). They protect the host organism against bacterial and fungal attacks by destroying the barrier function of the invading microbe's membrane (2). AMPs selectively disrupt the microbial cell membranes while maintaining the integrity of the host cell membranes. This selectivity is commonly believed to result from the different compositions of the two types of membranes. The most striking difference is that bacterial membranes are rich in anionic lipids but devoid of cholesterol, whereas red blood cell (RBC) membranes contain as much as 50 mol% cholesterol but few anionic lipids in the outer leaflet (3). However, how different membrane compositions affect the structure of AMPs is unknown.

The oligomeric assembly of AMPs is one structural aspect that may depend on the membrane composition. Existing models of antimicrobial mechanisms commonly assume aggregation of these peptides at some stages of their membrane-bound state (4). In the barrel-stave model (5) and the toroidal pore model (6, 7), the peptides cluster in the pores, whereas in the carpet model (8), densely aggregated peptides on the membrane surface thin the membrane until it micellizes. Yet direct determination of the aggregated structure of AMPs is scarce. We recently introduced a ¹⁹F spin diffusion NMR technique, centerband-only detection of exchange (CODEX), to determine the oligomeric number and intermolecular distances of membrane proteins in lipid bilayers (9). In this experiment, distance-dependent polarization transfer between singly ¹⁹F-labeled peptides reduces the equilibrium intensity

of a spin echo to 1/*n*, where *n* is the oligomeric number of the peptide. The time-dependent change of the echo intensity can be analyzed to extract intermolecular distances up to ≈ 15 Å (10). Using this method, we showed that the M2 peptide of influenza A virus forms tetramers in dimyristoylphosphatidylcholine (DMPC) bilayers (10), whereas protegrin-1 (PG-1), a β -hairpin AMP, has dimerized C strands in palmitoyloleoylphosphatidylcholine (POPC) bilayers (9).

Another distinction among various antimicrobial models is the degree of peptide insertion into lipid bilayers. The pore models postulate well inserted peptides, whereas the carpet model indicates surface-bound peptides. The depth of insertion can be determined by ¹H spin diffusion from the lipid chains to the protein (11). The greater the peptide-lipid separation, the slower the polarization transfer. Thus, a surface-bound membrane peptide exhibits slow spin diffusion from the lipid chain protons to the peptide, whereas an inserted peptide shows fast spin diffusion.

In this work, we use ¹⁹F and ¹H spin diffusion to determine the oligomeric structures of PG-1 in anionic membranes and cholesterol-containing neutral membranes. PG-1 is a disulfide-linked β -hairpin peptide originally isolated from pig leukocytes (12). It is active against a broad spectrum of pathogenic microorganisms, with minimum inhibitory concentrations of 0.1–2 μ M (13–15). In contrast, the concentrations causing 50% lysis of human erythrocytes are 12–80 μ M (14, 16) and are even higher for sheep and pigs (13). Thus PG-1 is at least 10-fold more selective against microbial cells than mammalian erythrocytes. The activity and the β -sheet conformation (17) of PG-1 are representative of many AMPs, such as human defensins (12). Thus, understanding the effect of membrane composition on PG-1's oligomeric structure may provide general insight into the origin of selective membrane disruption. We find that PG-1 adopts dramatically different oligomeric structures between the anionic membrane and the cholesterol-containing membrane, and the structure in the anionic membrane revises existing concepts of pore formation.

Results

Membrane Insertion of PG-1 in Anionic and Cholesterol-Containing Membranes. PG-1 structure was investigated in two lipid bilayers. The anionic palmitoyloleoylphosphatidyl ethanolamine and palmitoyloleoylphosphatidylglycerol (POPE/POPG) bilayer (mole ratio 3:1) mimics the bacterial inner membrane, whereas the neutral POPC/cholesterol bilayer (mole ratio 1.2:1) resembles the RBC

Author contributions: M.H. designed research; R.M., S.D.C., M.T., and A.J.W. performed research; R.M., R.I.L., and M.H. analyzed data; and M.H. wrote the paper.

The authors declare no conflict of interest.

This article is a PNAS direct submission.

Abbreviations: PG-1, protegrin-1; POPE, palmitoyloleoylphosphatidyl ethanolamine; POPG, palmitoyloleoylphosphatidylglycerol; POPC, palmitoyloleoylphosphatidylcholine; AMP, antimicrobial peptide; CODEX, centerband-only detection of exchange; P/L, peptide-lipid molar ratio; SNR, signal-to-noise ratio.

[†]To whom correspondence should be addressed. E-mail: mhong@iastate.edu.

© 2006 by The National Academy of Sciences of the USA

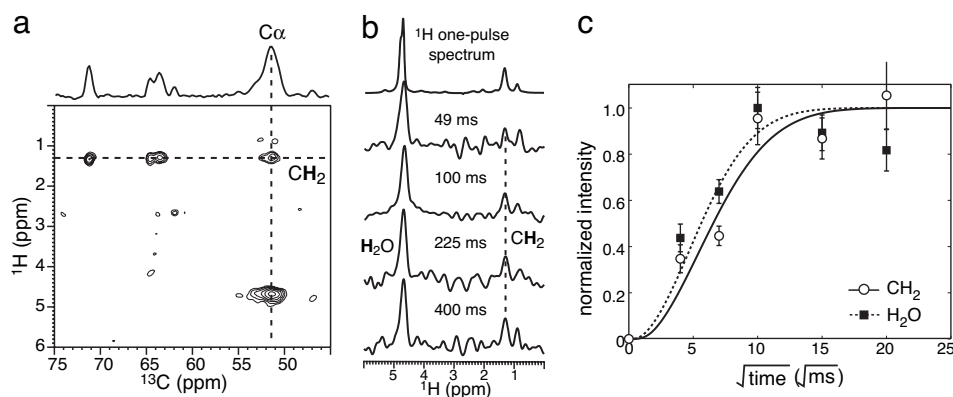


Fig. 1. ^1H spin diffusion data of PG-1 in POPE/POPG membrane. (a) 2D ^{13}C -detected ^1H spin diffusion spectrum of POPE/POPG (3:1) bilayers with ($^{13}\text{C}\alpha$ -Leu $_5$, $^{13}\text{C}'$ -Val $_{16}$) PG-1 at $t_m = 400$ ms. (b) Leu $\text{C}\alpha$ ^1H cross-sections for various t_m . The CH_2 and CH_3 signals are already visible at 100 ms. The ^1H one-pulse spectrum is shown at the top for comparison. (c) CH_2 (open circles) and H_2O (filled squares) buildup curves. The best fit for both is obtained with a distance of 2 ± 2 Å from the peptide by using $D_L = 0.012$ nm 2 /ms, $D_I = 0.00125$ nm 2 /ms, $D_W = 0.03$ nm 2 /ms, and $D_P = 0.3$ nm 2 /ms.

membrane. The high cholesterol concentration (45 mol%) of the latter is required to remove the PG-1 induced isotropic peak in the ^{31}P spectra, which is indicative of bilayer disruption into micelles or small vesicles (Fig. 7, which is published as supporting information on the PNAS web site).

A 2D ^{13}C -detected ^1H spin diffusion experiment was conducted to determine the depth of insertion of PG-1. Fig. 1a shows a representative 2D spectrum at $t_m = 400$ ms. The peptide is labeled with Val $_{16}$ $^{13}\text{C}'$ (172 ppm) and Leu $_5$ $^{13}\text{C}\alpha$ (51 ppm), thus cross-peaks between these and the lipid chain CH_2 (1.3 ppm) or CH_3 (0.9 ppm) signals indicate spin diffusion from the acyl chains to the peptide. Fig. 1b shows the ^1H cross-sections of Leu $_5$ $\text{C}\alpha$ at several t_m values. The lipid CH_2 peak is visible at t_m as short as 100 ms, indicating that PG-1 is in close proximity with the hydrophobic center of the membrane.

To extract distances, we analyze the cross-peak intensities as a function of t_m . The intensities are read off from peak heights in the 1D cross-sections, corrected for ^1H T_1 relaxation (≈ 700 ms for H_2O and CH_3 and ≈ 600 ms for CH_2), and normalized with respect to the maximum H_2O intensity at $t_m = 100$ ms. Because the equilibrium intensities of CH_2 and CH_3 peaks are only 36% and 14%, respectively, of the H_2O intensity (Fig. 1b, top spectrum), the CH_n ($n = 2, 3$) buildup curves are further scaled by these factors to account for the fact that, even at full-spin diffusion equilibrium, these cross-peaks are lower than the H_2O peak. The normalized CH_2 and

CH_3 intensities give the same buildup curves; thus, we analyze only the higher-sensitivity CH_2 data below.

Fig. 1c shows the buildup curves of the H_2O and CH_2 peaks of the anionic membrane. To fit the data, we calculate magnetization (M_i) transfer as a discrete process along the bilayer normal by using $\Delta M_i/\Delta t = -2\Omega M_i + \Omega M_{i+1} + \Omega M_{i-1}$, where the transfer rate Ω depends on the diffusion coefficients of the lipid (D_L), water (D_W), peptide (D_P), and peptide-lipid or peptide-water interface (D_I). D_L and D_P were estimated previously (11, 18) to be 0.012 nm 2 /ms and 0.3 nm 2 /ms, respectively. The buildup curve is determined by the thickness of the soft membrane between the source proton and the closest peptide residue, because its small D_L limits the rate of spin diffusion. This is the distance of interest. The interfacial D_I is an adjustable parameter in the simulation: it can be an order of magnitude smaller than D_L because of the transient nature of the peptide-lipid association. Fortunately, the effect of D_I on the buildup curve can be distinguished from the effect of the peptide-lipid separation (Fig. 8, which is published as supporting information on the PNAS web site).

Using $D_I = 1.25 \times 10^{-3}$ nm 2 /ms, we obtained the best fit for the CH_2 buildup with a peptide-lipid distance of ≈ 2 Å. Thus, PG-1 is in close contact with the acyl chains of the POPE/POPG bilayer. The H_2O buildup curve also fits to an ≈ 2 -Å distance, indicating that PG-1 also contacts the membrane surface. Because of the approximate nature of D_L and D_I values, the uncertainties of these distances are approximately ± 2 Å.

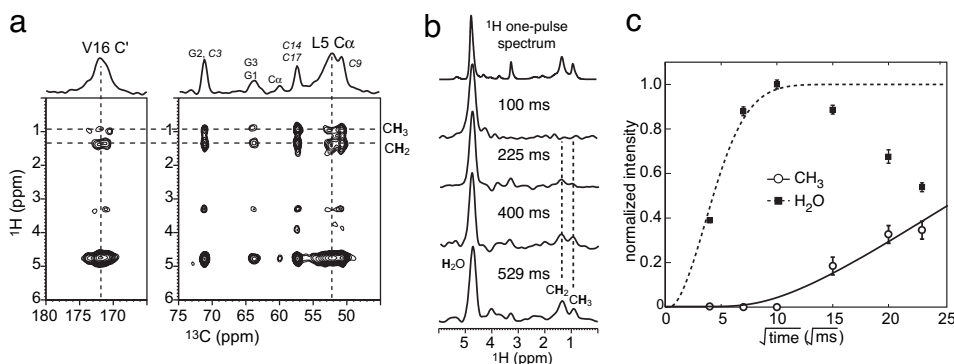


Fig. 2. ^1H spin diffusion data of PG-1 in POPC/cholesterol membrane. (a) 2D ^{13}C -detected ^1H spin diffusion spectra of POPC/cholesterol (1.2:1) membranes with ($^{13}\text{C}\alpha$ -Leu $_5$, $^{13}\text{C}'$ -Val $_{16}$) PG-1 at $t_m = 529$ ms. Assignment for lipid and cholesterol (italic) ^{13}C peaks is indicated in addition to the two peptide labels. (b) Combined ^1H cross-sections for Leu $_5$ - $\text{C}\alpha$ and Val $_{16}$ - $^{13}\text{C}'$. The CH_2 and CH_3 peaks are absent until 225 ms. The ^1H one-pulse spectrum is shown at the top. (c) CH_3 (open circles) and H_2O (filled squares) buildup curves, best fit by distances of 20 ± 2 Å and 2 ± 2 Å, respectively.

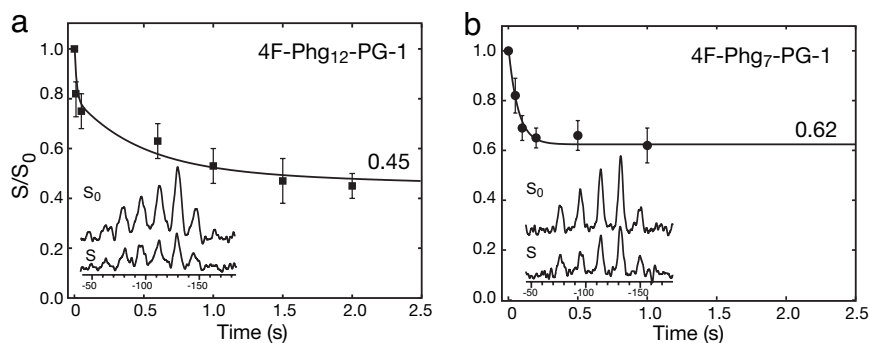


Fig. 3. ^{19}F CODEX data of 4F-Phg₁₂-PG-1 (a) and 4F-Phg₇-PG-1 (b) in POPE/POPG bilayers. S_0 and S spectra at $t_m = 1$ s are shown for each sample. The data in a is best fit with a 60%:40% mixture of a 9.0 ± 0.5 Å and a 5.0 ± 0.5 Å nearest-neighbor distance. The best fit for b is obtained with a 75%:25% mixture of a dimer with a distance of 6.5 Å and a monomer.

The ^1H spin diffusion of PG-1 in POPC/cholesterol bilayers differs dramatically from the anionic membrane case. Although the CH_2 -peptide cross-peak is clearly visible at 529 ms (Fig. 2a), it is completely absent until 225 ms (Fig. 2b). This result suggests that PG-1 does not insert into the hydrophobic part of the POPC/cholesterol bilayer. In contrast, the H_2O buildup is rapid, reaching a plateau at 100 ms. The T_1 - and equilibrium-intensity-corrected buildup curves (Fig. 2c) quantitatively exhibit the different rates of spin diffusion from these two types of protons. The decay of the H_2O intensity at longer times is attributable to net polarization loss to PG-1 and the lipids. Using the 1D lattice model, we find the best fit to the CH_3 data at 20 ± 2 Å and the H_2O data at 2 ± 2 Å, indicating that PG-1 lies on the surface of the bilayer, away from the center of the membrane. For the CH_3 curve, a small D_1 of 2.5×10^{-4} nm^2/ms was required to reproduce the small slope of the buildup, whereas the large distance reproduces the slow onset of spin diffusion.

PG-1 Oligomerization in Anionic Membranes. To determine the oligomeric structure of PG-1, we carried out the ^{19}F CODEX experiment. Two ^{19}F -labeled peptides were used: one with 4- ^{19}F -Phg₁₂ near the β -turn on the C-terminal strand (C strand) and the other with 4- ^{19}F -Phg₇ on the N-terminal strand (N strand). The replacement of Phe by Phg, which does not have a β - CH_2 group, removes χ_1 torsional freedom, thus eliminating one possible mechanism of motional exchange. Antimicrobial assays indicate that Phg-containing PG-1 has very similar activities as wild-type PG-1 (Fig. 9, which is published as supporting information on the PNAS web site). The remaining motion of the Phg side chain, 180° flip of the ring, does not change the ^{19}F position or the ^{19}F chemical-shift tensor orientation, thus cannot cause exchange during t_m . To minimize possible slow backbone motion, which could interfere with spin diffusion, the experiments were carried out at temperatures well below the phase-transition temperature (≈ 291 K) of the POPE/POPG bilayer (225 K for Phg₁₂-PG-1 and 233 K for Phg₇-PG-1).

Fig. 3 shows normalized exchange intensities of 4F-Phg₁₂-PG-1 (Fig. 3a) and 4F-Phg₇-PG-1 (Fig. 3b) in POPE/POPG membranes. Phg₁₂-PG-1 shows an equilibrium value, $(S/S_0)_{\text{eq}}$, of 0.45, whereas Phg₇-PG-1 exhibits a higher $(S/S_0)_{\text{eq}}$ of 0.62. Thus, each ^{19}F spin on average experiences couplings to one other ^{19}F within a radius of ≈ 15 Å. The Phg₁₂ $(S/S_0)_{\text{eq}}$ of <0.5 suggests that spin diffusion to a third, more remote ^{19}F spin is partly detected. On the other hand, the Phg₇ $(S/S_0)_{\text{eq}}$ of >0.5 is possible only if some monomers [with $(S/S_0)_{\text{eq}} = 1$] coexist with oligomers. The simplest oligomer is a dimer, in which case a dimer fraction of 75% and a monomer fraction of 25% are required to give the observed $(S/S_0)_{\text{eq}} = 0.62$.

In addition to the different $(S/S_0)_{\text{eq}}$, the two 4F-Phg residues

show different decay constants (τ_{SD}). Phg₁₂ exhibits a τ_{SD} of 1.2 ± 0.4 s mixed with an initial fast component of 0.008 ± 0.002 s, whereas Phg₇-PG-1 has a single-exponential τ_{SD} of 0.06 ± 0.01 s. To extract quantitative distances, we simulated the t_m -dependent curves by using a rate-matrix approach. The t_m -dependence of diffusion among n spins is described by $\bar{M}(t_m) = e^{-\bar{K}t_m}\bar{M}(0)$, where \bar{K} is an n -dimensional exchange matrix containing the rate constants k_{ij} . These rate constants depend on the F-F dipolar couplings, ω_{ij} , and a spectral overlap integral, $F(0)$, between the exchanging spins (19). With a known $F(0)$, dipolar couplings can be extracted from curve fitting, from which distances can be derived as $\omega_{ij} = (\gamma^2\hbar\mu_0/4\pi)/r_{ij}^3$. We recently determined the ^{19}F $F(0)$ value to be $37 \mu\text{s}$ at 8 kHz magic angle spinning (MAS), by using model compounds with known crystal structures (10).

Using this rate-matrix approach, we find the Phg₇ data are best fit by a 75%:25% mixture of a two-spin cluster with a distance of 6.5 Å and an isolated spin (Fig. 3b). For Phg₁₂, a 60%:40% mixture of a distance of 9.0 ± 0.5 Å and 5.0 ± 0.5 Å fit the data well. The mixture is necessitated by the biexponentiality of the decay: the short distance fits the fast initial decay, whereas the long distance fits the slow decay. Note that these ^{19}F - ^{19}F distances are more precise (± 0.5 Å) than the ^1H spin diffusion distances.

Because the Phg₇ data indicates 75% dimerization of the N strand, the $(S/S_0)_{\text{eq}}$ of <0.5 for Phg₁₂ is most likely attributable to the presence of an additional 4F-Phg₁₂ ≈ 15 Å away on a third hairpin. Indeed, simulations show that a four-spin cluster with the next-nearest-neighbor distance of 15 Å in addition to the nearest distance of 9 Å or 5 Å better reproduces $(S/S_0)_{\text{eq}}$. An odd-number cluster is ruled out by the double-stranded nature of the hairpin and the average cluster size of two for each ^{19}F label. On the other hand, even-number clusters larger than four are possible because the detection limit is 15 Å.

To verify whether residual motion contributes to the fast exchange at short times (Fig. 3a), we measured the Phg₁₂ 50-ms CODEX at 225 K, 230 K, and 240 K. The 240 K data gave a significantly lower S/S_0 of 0.60 ± 0.06 , indicating the presence of motional exchange. However, at 230 K, $S/S_0 = 0.72 \pm 0.05$, which is indistinguishable from the value of 0.75 ± 0.07 at 225 K. Thus, the main mechanism of exchange at 225 K is spin diffusion.

Taking the majority conformer for Phg₁₂ (60%) and Phg₇ (75%), we consider the structure of the dominant fraction, 45% ($= 60\% \times 75\%$), of PG-1 in POPE/POPG bilayers. Only four molecules (A–D) are shown in Fig. 4a for clarity. The β -hairpins pack in parallel. The C strand interfaces satisfy the Phg₁₂^{A,C}–Phg₁₂^{B,D} F–F distance of 9 Å, as well as previously measured Val₁₆ C'–Phe₁₂ 4F distances of 9.3 Å and 16 Å, and Cys₁₅ C'–Cys₁₅ H^N distances of 2.5 Å and 6.5 Å (20). The N strand is constrained by only the Phg₇–Phg₇ distance (6.5 Å), thus multiple packing

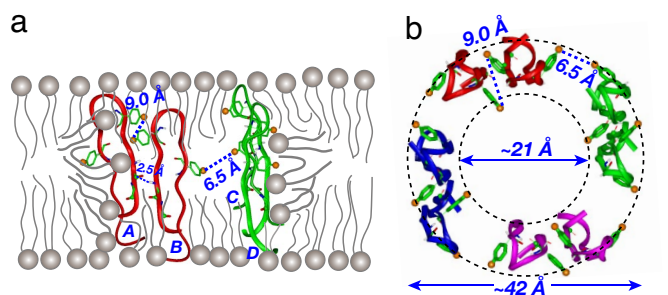


Fig. 4. Model of PG-1 β -barrel in POPE/POPG membrane. (a) Side view. The two dimers are rotated from each other along the molecular axis. Pore-lining lipids are orientationally disordered and have chain upturns. (b) Top view. An octameric PG-1 complex surrounds a water pore of ≈ 21 -Å diameter. The outer diameter of the pore is ≈ 42 Å.

arrangements are possible. These can be distinguished by whether the dimer CD is only translated from the dimer AB or whether the dimer CD is both rotated and translated from the dimer AB. For the former, the outermost N strands are isolated unless more peptides are oligomerized. To satisfy the 75% dimer fraction, at least eight hairpins must be packed in a sheet to have the right fraction of monomers. Such a flat β -sheet is unlikely to be inserted into the 2D membrane as dictated by the ^1H spin diffusion data. Thus, the motif where the dimers are rotated from each other around the long axis of the molecule is more likely. The resulting curved $(\text{NCCN})_n$ ($n > 1$) multimer suggests a β -barrel that closes onto itself, satisfying the two-spin requirement for each ^{19}F label as well as forming hydrogen bonds for each β -strand. This β -barrel surrounds a water pore, whose diameter can be estimated from size-dependent blockage of PG-1 pores by polyethylene glycol (PEG) across *Escherichia coli* inner membranes (21, 22). PEG molecules with hydrodynamic radii (R_{H}) up to 0.94 nm allowed membrane permeabilization, whereas those with $R_{\text{H}} = 1.05$ nm blocked permeabilization by PG-1 (R.I.L., unpublished data). Thus, the diameter of the water pore is at most ≈ 21 Å, which is possible with 8 or 10 peptides (Fig. 4b).

The $(\text{NCCN})_n$ ($n > 1$) β -barrel is the dominant component of a heterogeneous mixture. The other oligomeric structures include a 30% ($= 40\% \times 75\%$) fraction of multimers with more compact C strand interfaces (Phg₁₂-Phg₁₂, 5 Å) and a 25% fraction of NCCN dimers without an N strand interface. The latter is consistent with PG-1 fibrilization data indicating that the N strand interface is looser than the C strand interface, perhaps as a result of the cationic Arg₄ in the middle of the hydrophobic N strand (23).

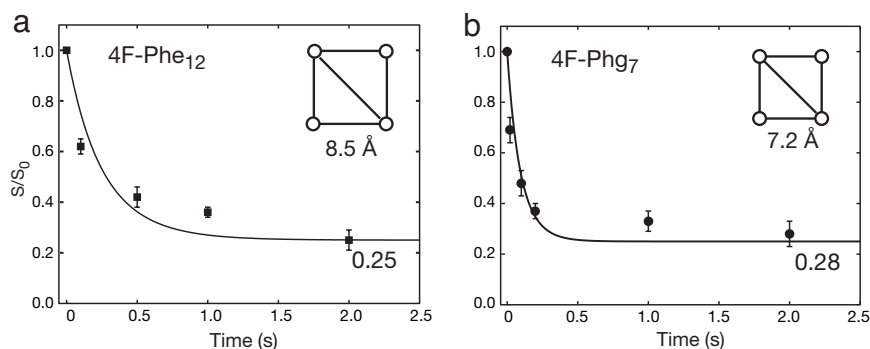


Fig. 5. ^{19}F CODEX data of 4F-Phe₁₂-PG-1 (a) and 4F-Phg₇-PG-1 (b) in POPC/cholesterol bilayers. Both show $(S/S_0)_{\text{eq}}$ of ≈ 0.25 , indicating four-spin clusters. Simulations performed with a square geometry gave a side length of 8.5 Å for a and 7.2 Å for b.

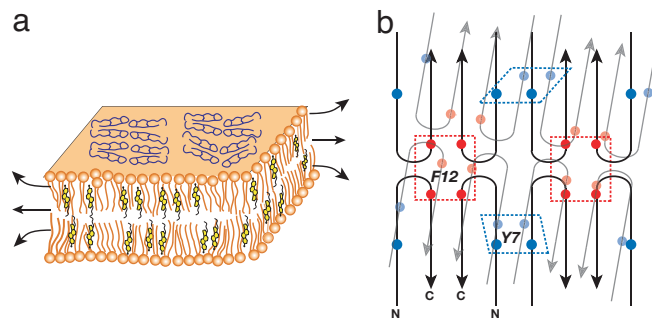


Fig. 6. A model of PG-1 structure in POPC/cholesterol bilayers. (a) PG-1 aggregates into β -sheets on the membrane surface. Cholesterol is embedded in the acyl chain and glycerol regions, exerting a negative curvature strain that prevents PG-1 insertion. (b) The β -sheets yield four-spin clusters for Phe₁₂ and Phg₇. The molecules in the two β -sheets are not aligned.

PG-1 Oligomerization in POPC/Cholesterol Membranes. ^{19}F spin diffusion of PG-1 in POPC/cholesterol bilayers differs significantly from the case in the anionic membrane. $(S/S_0)_{\text{eq}}$ values of ≈ 0.25 are observed for both Phe₁₂-PG-1 and Phg₇-PG-1 (Fig. 5), indicating that each ^{19}F resides in a four-spin cluster. The Phe₁₂ decay, acquired at 230 K and a peptide-lipid molar ratio (P/L) of 1:8, was reproduced at $t_{\text{m}} = 0.5$ s and 2 s on Phg₁₂-PG-1 at 225 K and P/L = 1:12.5. The use of Phg and the lower temperature both reduce the possibility of motional exchange, thus they should increase S/S_0 if motion were present in the 1:8 sample. The lower peptide concentration also will increase S/S_0 if oligomerization is incomplete at 1:12.5. The fact that identical S/S_0 values were found is strong proof that the measured exchange is purely attributable to spin diffusion, and the average oligomeric size of four is constant between the two concentrations. We also tested the exchange mechanism of Phg₇-PG-1 in the POPC/cholesterol/trehalose membrane. The experiment was repeated at 248 K versus 233 K for the full experiment. The S/S_0 values remained the same at $t_{\text{m}} = 20$ ms and 1 s, indicating that no slow motion is present between 233 K and 248 K.

The CODEX decays were simulated assuming a symmetric tetramer model, so that the 4×4 rate matrix depends only on one distance, the length of the square (Fig. 5). For Phe₁₂, the best-fit distance is 8.5 Å, whereas the Phg₇ data gives a distance of 7.2 Å.

To obtain tetrameric clusters for both Phe₁₂ and Phg₇, the most likely packing motif is β -sheet on the surface of the POPC/cholesterol bilayer (Fig. 6a). The Phe₁₂ cluster may be formed by two apposing NCCN dimers where four β -turns aggregate (Fig. 6b). The Phg₇ cluster cannot easily be formed in one β -sheet because only two N strands can pack closely in a plane. Thus, two β -sheets may be stacked to produce the four-spin cluster (Fig. 6b).

Discussion

The above experiments indicate that PG-1 has distinct oligomeric structures and insertion states in bacteria-mimetic anionic membranes and RBC-mimetic POPC/cholesterol membranes. In the anionic membrane, PG-1 contacts both the lipid headgroup and acyl chains and thus is well inserted. The peptide assembles into $(\text{NCCN})_n$ multimers whose like-stranded interfaces are constrained not only by F-F distances but also by previously measured heteronuclear distances in POPC bilayers (20), which indicated parallel packed and hydrogen-bonded C strands. Such a hydrogen-bond stabilized $(\text{NCCN})_n$ multimer strongly suggests the formation of a β -barrel.

Pore formation by PG-1 is known from a number of experiments. Conductance measurements indicated that PG-1 induces weakly anion-selective channels in both planar bilayers and *Xenopus* oocytes (24, 25). Scanning electron micrographs showed multiple, annular structures on the outer membranes of *Neisseria gonorrhoeae* (26) and other proteogrin-treated Gram-negative bacteria. Neutron diffraction patterns indicate that PG-1-containing fluid dimyristoylphosphatidylcholine (DMPC) membranes have D_2O -filled pores that become correlated across different bilayers as the membrane is dehydrated or cooled (27). None of these studies, however, yielded the molecular structure of PG-1 at the pores. The current solid-state NMR data fills this gap. Based on the intermolecular distances and the estimated pore inner diameter of 21 Å, the PG-1 β -barrel most likely contains four to five NCCN dimers, resulting in a pore outer diameter of ≈ 42 Å.

A well defined oligomeric β -barrel of PG-1 contradicts an important feature of the toroidal pore model, in which the lipids in one leaflet bend toward the other to make the two leaflets continuous (7, 28). One hypothesis of the model is that the peptides in the pores are monomeric and act as fillers to relieve membrane bending stress (7). This hypothesis is inconsistent with the current data. Instead, the PG-1 β -barrel has tight C strand interfaces, where the shortest intermolecular distance is 2.5 Å between Cys₁₅ C' and Cys₁₅ H^N (20). Even the N strand interfaces, with fewer distance constraints so far, have a remarkably short Phg₇-Phg₇ distance (6.5 Å) and a high percentage (75%) of dimerization. The extensive oligomerization is fully consistent with the lack of PG-1 mobility in POPC membranes (29), which interact with PG-1 similarly as POPE/POPG membranes (30). The PG-1 β -barrel resembles the multimeric pore proposed for HNP-2, a human β -defensin containing similar Cys-linked β -strands (31). The HNP-2 annulus, surrounding a pore with a maximum diameter of 25 Å, was hypothesized to contain six to eight dimers, whose amphipathic structure had been observed in the crystalline, nonlipidic state (32).

With the β -barrel forming the core of the toroidal pore, we propose that it is the lipids rather than the peptide that act as fillers of the pore. The pore-lining lipids have high orientational disorder (33). ³¹P lineshapes of glass-plate aligned POPE/POPG bilayers indicate a nonlamellar fraction of $\approx 50\%$ at P/L = 1:25 (30). At P/L = 1:12.5, the disordered fraction should be even higher. However, the original proposal that the pore lining is covered completely by lipid headgroups contradicts the ¹H spin diffusion data showing close contact between the lipid chains and the peptide. It also disagrees with the negative curvature of POPE, whose headgroup is smaller than the chains in the cross-sectional area. To resolve these conflicts, we propose that the lipids lining the pore have significant chain upturns and residual orientations parallel to the pore axis (Fig. 4a). Chain upturns have been observed even in lamellar bilayers (34) and may be quite common in defect regions of the membrane. Moreover, because the PG-1 barrel is only ≈ 30 -Å thick, whereas the POPE/POPG membrane is ≈ 45 -Å thick, the lipids above and below the β -barrel may be packed in such a way as to allow both headgroup and chain contacts with the peptide. Evidence that the pore-rich membrane is not thinned by PG-1 is found in ²H quadrupolar spectra of *d*₃₁-POPC (33). A

reduction of ²H quadrupolar couplings is known to denote membrane thinning. We found that the ²H splittings are unchanged by PG-1 binding, suggesting that the POPC membrane is not significantly thinned by PG-1.

The 25% of PG-1 that forms NCCN dimers are likely inserted into the residual lamellar portion of the bilayer. The presence of small dimers is understandable because aggregation is a cooperative, concentration-dependent phenomenon (35). The dimers may act as nucleating units for the β -barrels. C strand dimers of PG-1 are present even in dodecylphosphocholine micelles, indicating the strong oligomerization propensity of this more hydrophobic strand (36).

In contrast to the anionic membrane, PG-1 does not insert into the POPC/cholesterol bilayer. The shortest distance from PG-1 to the lipid methyl protons is ≈ 20 Å. The CH₃ buildup curve is very similar to that of a DNA-lipid complex, where the anionic DNA is sandwiched between bilayers with cationic headgroups, 20 Å from the bilayer center (11). The surface location of PG-1 in POPC/cholesterol bilayers is reasonable, because cholesterol inserts into the hydrophobic and glycerol regions of the bilayer (37), and thus should exert a negative curvature strain that counters PG-1 insertion (Fig. 6a). The rigid sterol rings of cholesterol also help to reduce the membrane elasticity, making it more difficult for the bilayer to deform to accommodate PG-1 insertion. Lamellar x-ray diffraction data suggest that PG-1 undergoes a transition from a surface-bound state to an inserted state near P/L = 1:40 in cholesterol-free phosphocholine bilayers (38). Thus, the fact that PG-1 remains surface-bound at a much higher concentration in POPC/cholesterol bilayers is interesting and indicates that peptide insertion is sensitively influenced by the membrane composition.

The four-spin cluster of Phg₇ requires the local stacking of two β -sheets because only two N strands can pack closely in each sheet. The β -sheets can be small, containing as few as eight peptides. The hairpins in the two sheets must not be aligned, in order that the Phg₁₂ cluster size does not extend appreciably beyond four. The two β -sheets may pack between the bilayers: at 35–50 wt % H₂O, the hydration layer in multilamellar POPC/cholesterol membranes is ≈ 25 -Å thick (39), enough to accommodate two but not more β -sheets. More likely, however, the peptide may aggregate on the outer surface of the multilamellar liposome in a more disordered fashion. In either case, the effective surface concentration of the peptide is reduced by stacking, which decreases the lytic ability of PG-1 (40).

It should be pointed out that PG-1's hemolytic activities differ among mammals. For example, it is substantially more active against human RBC than those of ruminants (cattle and sheep) or pigs (13). This difference may reflect the interspecies variation of erythrocyte membranes, such as the asymmetric distribution of phospholipids in the outer and inner leaflets, their different phospholipid compositions, and the presence of embedded (glyco)proteins (41).

In both the β -barrel and the β -sheet structure, the Arg-rich β -turn of the peptide clusters together, causing as many as 6 or 12 Args to aggregate. Clustering of like-charged ions, although counterintuitive at first, is common in ionic polymers such as Nafion (42, 43). In PG-1, the Arg clusters are most likely solvated by the phosphate headgroups. Indeed, guanidinium-phosphate complexes are known to be very stable because of multiple hydrogen bonds (44, 45).

The PG-1 β -barrel and β -sheet structures proposed in this article for the anionic versus neutral cholesterol-containing membranes can be refined by measuring more intermolecular distance constraints, especially at the N strand interface. Heteronuclear distance experiments involving high-frequency nuclei such as ¹H and ¹⁹F will be useful for this purpose. In comparison, structural information about lipid packing around the peptide will necessarily remain statistical because of the inherent disorder of the lipid membrane.

Materials and Methods

Materials. PG-1 (NH₂-RGGRLCYRRRRCVVCVGR-CONH₂) was synthesized by using Fmoc solid-phase chemistry and purified by reverse-phase HPLC as described in ref. 33. Peptides with 4F-Phg contain a racemic mixture of D and L forms (46), which were separated by HPLC. The L fraction was identified by using Marfey's reagent (47), then purified by size-exclusion chromatography to remove trifluoroacetate ions, which interfere with the ¹⁹F experiments. The peptides were dialyzed exhaustively, and their purity was assessed by MALDI-TOF mass spectrometry, analytical HPLC, and ¹⁹F solution NMR.

Membrane Sample Preparation. PG-1 and lipids were mixed initially either in chloroform or in aqueous solution. For the former, the organic solvent was vacuum-dried, and then the membrane film was hydrated to 35 wt % water. For the latter, large unilamellar lipid vesicles were prepared by freeze-thawing, the peptide was mixed with the vesicle solution, and then the mixture was ultracentrifuged to give a membrane pellet containing ≈50 wt % water. Cholesterol-containing samples were prepared in both ways and gave the same oligomeric state based on the CODEX experiment. The POPE/POPG samples were prepared in the aqueous phase, and PG-1 binding was found to be quantitative (>90%) by UV/Vis absorption.

For membranes containing Phg₇-PG-1, 20 wt % trehalose was added, and the membrane mixtures were lyophilized for the NMR experiments. Trehalose preserves the lamellar structure of dry membranes in the absence of water by replacing the hydration water around the lipid headgroups (48). Small amounts of trehalose raise the phase-transition temperature of the membrane compared with the hydrated bilayer, thus reducing lipid motion (49) and allowing the CODEX experiments to be conducted at milder temperatures (M.T., unpublished data). Experiments on hydrated and trehalose-containing POPC/PG-1 membranes confirmed that the oligomeric state of PG-1 is the same between the two.

All membrane samples have a P/L of 1:12.5, except for the 4F-Phe₁₂-PG-1 sample in the POPC/cholesterol bilayer, which has P/L = 1:8. Only phospholipids, not cholesterol and trehalose, are included in the mole ratio calculation.

Solid-State NMR Spectroscopy. NMR experiments were carried out on a Bruker (Karlsruhe, Germany) DSX-400 spectrometer operating at a resonance frequency of 400.5 MHz for ¹H, 376.8 MHz for

¹⁹F, and 100.7 MHz for ¹³C. The ¹⁹F experiments were conducted on a H/F/X probe at spinning speeds of 6.5, 7, and 8 kHz. Cross-polarization contact times were 0.2–0.5 ms. ¹³C and ¹⁹F chemical shifts were referenced externally to the α-glycine ¹³C' signal at 176.49 ppm and the Teflon ¹⁹F signal at –122 ppm, respectively.

2D ¹³C-detected ¹H spin-diffusion experiments were conducted at 298 K at 4 or 5 kHz magic angle spinning. After ¹H evolution, a mixing time (*t_m*) of 16–529 ms was applied to transfer ¹H polarization from the mobile lipids and water to the peptide, which then was detected through ¹³C. To ensure that only the mobile lipid and water polarization served as the source of spin diffusion, we suppressed the rigid peptide polarization by a ¹H T₂ relaxation filter of 2 ms before ¹H chemical-shift evolution and spin diffusion. 1D ¹³C spectra obtained without ¹H spin diffusion confirmed that the 2-ms ¹H T₂ filter completely suppressed the peptide signals while retaining the lipid signals (Fig. 10, which is published as supporting information on the PNAS web site).

In the CODEX experiments, ¹⁹F chemical shift anisotropy (CSA) was recoupled before and after *t_m* by using one π-pulse-containing rotor period. The recoupling time is 2τ_r. At 6.5–8 kHz magic angle spinning, and with a ¹⁹F CSA (δ = δ_{zz} – δ_{iso}) of 52 ppm, this amounts to 2πδ_r2δ_r = 10π – 12π, which is large enough to detect orientation differences as small as 20° (50). For each *t_m*, a control experiment (S₀) was carried out in which the z filter (10 μs) and *t_m* were interchanged from those of the exchange experiment (S). The normalized intensity, S/S₀, indicates spin exchange without ¹⁹F T₁ relaxation and is monitored as a function of *t_m*.

The uncertainties of S/S₀, ε_{S/S₀}, were propagated from the signal-to-noise ratios (SNR) of the S₀ and S spectra according to ε_{S/S₀} = (S/S₀)[ε_{S₀}² + ε_S²]^{1/2}, where ε is 1/SNR (20). Sideband intensities were included in the SNR calculation by using SNR_{total} = SNR₀/(ΣP_i²/P₀²), where P₀ is the intensity of the highest peak of the spectrum.

PG-1 oligomeric structures were built and visualized in Insight II, starting from the solution-NMR monomer structure (17). Phe₁₂ and Tyr₇ were changed to L-Phg by replacing the side chains with a benzene ring. Recently determined C-F, C-H, and C-N distances (20) and the F-F distances are combined to constrain the intermolecular interfaces.

This work is supported by National Institutes of Health Grants GM-066976 (to M.H.) and AI-37945 (to A.J.W. and R.I.L.).

- Zaslouff M (2002) *Nature* 415:389–395.
- Hancock RE, Lehrer R (1998) *Trends Biotechnol* 16:82–88.
- Rouser G, Nelson GJ, Fleischer S, Simon G (1968) in *Biological Membranes: Physical Fact and Function*, ed Chapman D (Academic, New York).
- Bechinger B (1999) *Biochim Biophys Acta* 1462:157–183.
- He K, Ludtke SJ, Worcester DL, Huang HW (1996) *Biophys J* 70:2659–2666.
- Matsuzaki K (1998) *Biochim Biophys Acta* 1376:391–400.
- Ludtke SJ, He K, Heller WT, Harroun TA, Yang L, Huang HW (1996) *Biochemistry* 35:13723–13728.
- Pouny Y, Rapaport D, Mor A, Nicolas P, Shai Y (1992) *Biochemistry* 31:12416–12423.
- Buffly JJ, Waring AJ, Hong M (2005) *J Am Chem Soc* 127:4477–4483.
- Luo W, Hong M (2006) *J Am Chem Soc* 128:7242–7251.
- Huster D, Yao XL, Hong M (2002) *J Am Chem Soc* 124:874–883.
- Kokryakov VN, Harwig SS, Panyutich EA, Shevchenko AA, Aleshina GM, Shamova OV, Korneva HA, Lehrer RI (1993) *FEBS Lett* 327:231–236.
- Bellm L, Lehrer RI, Ganz T (2000) *Exp Opin Invest Drugs* 9:1731–1742.
- Tam JP, Wu C, Yang JL (2000) *Eur J Biochem* 267:3289–3300.
- Steinberg DA, Hurst MA, Fujii CA, Kung AHC, Ho JF, Cheng FC, Loury DJ, Fiddes JC (1997) *Antimicrob Agents Chemother* 41:1738–1742.
- Yasin B, Pang M, Turner JS, Cho Y, Dinh NN, Waring AJ, Lehrer RI, Wagar EA (2000) *Eur J Clin Microbiol Infect Dis* 19:187–194.
- Fahrner RL, Dieckmann T, Harwig SS, Lehrer RI, Eisenberg D, Feigon J (1996) *Chem Biol* 3:543–550.
- Clauss J, Schmidt-Rohr K, Spiess HW (1993) *Acta Polymer* 44:1–17.
- Vanderhart DL (1987) *J Magn Reson* 72:13–47.
- Mani R, Tang M, Wu X, Buffly JJ, Waring AJ, Sherman MA, Hong M (2006) *Biochemistry* 45:8341–8349.
- Lehrer RI, Barton A, Ganz T (1988) *J Immunol Methods* 108:153–158.
- Ternovsky VI, Okada Y, Sabirov RZ (2004) *FEBS Lett* 576:433–436.
- Tang M, Waring AJ, Hong M (2005) *J Am Chem Soc* 127:13919–13927.
- Mangoni ME, Aumelas A, Charnet P, Roumestand C, Chiche L, Despau E, Grassy G, Calas B, Chavanieu A (1996) *FEBS Lett* 383:93–98.
- Sokolov Y, Mirzabekov T, Martin DW, Lehrer RI, Kagan BL (1999) *Biochim Biophys Acta* 1420:23–29.
- Qu XD, Harwig SS, Oren AM, Shafer WM, Lehrer RI (1996) *Infect Immun* 64:1240–1245.
- Yang L, Weiss TM, Lehrer RI, Huang HW (2000) *Biophys J* 79:2002–2009.
- Matsuzaki K, Murase O, Fujii N, Miyajima K (1996) *Biochemistry* 35:11361–11368.
- Buffly JJ, Waring AJ, Lehrer RI, Hong M (2003) *Biochemistry* 42:13725–13734.
- Mani R, Buffly JJ, Waring AJ, Lehrer RI, Hong M (2004) *Biochemistry* 43:13839–13848.
- Wimley WC, Selsted ME, White SH (1994) *Protein Sci* 3:1362–1373.
- Hill CP, Yee J, Selsted ME, Eisenberg D (1991) *Science* 251:1481–1485.
- Yamaguchi S, Hong T, Waring A, Lehrer RI, Hong M (2002) *Biochemistry* 41:9852–9862.
- Huster D, Gawrisch K (1999) *J Am Chem Soc* 121:1992–1993.
- Schwarz G, Stankowski S, Rizzo V (1986) *Biochim Biophys Acta* 861:141–151.
- Roumestand C, Louis V, Aumelas A, Grassy G, Calas B, Chavanieu A (1998) *FEBS Lett* 421:263–267.
- Villalain J (1996) *Eur J Biochem* 241:586–593.
- Huang HW (2000) *Biochemistry* 39:8347–8352.
- Rand RP, Parsegian VA (1989) *Biochim Biophys Acta* 988:351–376.
- Wieprecht T, Apostolov O, Beyermann M, Seelig J (2000) *Biochemistry* 39:442–452.
- Virtanen JA, Cheng KH, Somerharju P (1998) *Proc Natl Acad Sci USA* 95:4964–4969.
- Mauritz KA, Moore RB (2004) *Chem Rev* 104:4535–4585.
- Gierke TD, Munn GE, Wilson FC (1981) *J Polymer Sci* 19:1687–1704.
- Sakai N, Mareda J, Matile S (2005) *Acc Chem Res* 38:79–87.
- Schug KA, Lindner W (2005) *Chem Rev* 105:67–114.
- Afonin S, Glaser RW, Berditchevskaia M, Wadhvani P, Guhrs KH, Mollmann U, Perner A, Ulrich AS (2003) *ChemBioChem* 4:1151–1163.
- Marfey P (1984) *Carlsberg Res Commun* 49:591.
- Crowe JH, Crowe LM, Chapman D (1984) *Science* 223:701–703.
- Lee CW, Das Gupta SK, Mattai J, Shipley G, Abdel-Mageed OH, Makriyannis A, Griffin RG (1989) *Biochemistry* 28:5000–5009.
- deAzevedo ER, Bonagamba TJ, Hu W, Schmidt-Rohr K (1999) *J Am Chem Soc* 121:8411–8412.